Ferroelectric and Anti-Ferroelectric Hafnium Zirconium Oxide: Scaling Limit, Switching Speed and Record High Polarization Density

X. Lyu[1], M. Si[1,*], X. Sun[2], M. A. Capano[1], H. Wang[2], and P. D. Ye[1,**]

[1]School of Electrical and Computer Engineering and [2]School of Materials Science and Engineering, Purdue University, West Lafayette, IN 47907, U.S.A. *Email: msi@purdue.edu, **Email: yep@purdue.edu

Abstract

The ferroelectric (FE) and anti-ferroelectric (AFE) properties of hafnium zirconium oxide (HZO) are investigated systematically down to 3 nm. The ferroelectric polarization, switching speed and the impact of atomic layer deposited (ALD) tungsten nitride (WN) electrodes are studied. Record high remnant polarization (P_r) on FE HZO and record high saturation polarization (P_S) on AFE HZO are achieved with WN electrodes, especially in ultrathin sub-10 nm regime. A high dielectric constant of 30.4 is achieved on AFE HZO. The polarization switching speed of FE and AFE HZO, associated with C-V frequency dispersion, are also studied. For the first time, it is found polarization switching speed is faster in AFE HZO than FE HZO, suggesting AFE-FET could be more promising for high speed memory devices.

Introduction

FE HfO_2 is a very promising thin film oxide for ferroelectric memory (FeRAM) applications, especially for the FET-type FeRAM, because of its CMOS compatible ALD process [1, 2], fast read/write speed [3-5], long retention time [2, 6] and high endurance [7, 8]. The scaling down of FE HfO_2 becomes extremely important to reduce the supply voltage of Fe-FETs and thereby reduce the power consumption. It is well known the ferroelectricity in FE thin films is highly thickness dependent in terms of P_r, coercive electric field (E_c), polarization switching speed, *etc.* Such FE properties are also strongly related with processing conditions. However, there are few reports on the scaling performance of FE HfO_2 down to deep sub-10 nm [9, 10] and no systematic studies on both FE and AFE HZO at the same scaling limit.

In this work, the FE and AFE scaling properties of HZO are investigated systematically by P-V, C-V and fast pulse I-V measurements. Record high P_r of 13.8 μC/cm^2 is achieved at 4 nm FE HZO with Hf:Zr=1:1. Record high P_S of 28.1 μC/cm^2 is achieved at 4.5 nm AFE HZO with Hf:Zr=1:3, also with high dielectric constant of 30.4. WN electrode is found to improve the FE performance of HZO significantly. Through C-V and pulse I-V measurements, AFE HZO is confirmed to operate at a higher speed than FE HZO, indicating AFE-gated transistor is more promising for high-speed memory devices.

Experimental

TiN, WN and HZO were deposited by ALD. TiN was deposited at 250 °C, using TDMAT and NH_3 as the Ti and N precursors. WN was deposited at 400 °C, using BTBMW and NH_3 as the W and N precursors. $Hf_{1-x}Zr_xO_2$ film was deposited at 200 °C, using TDMAHf, TDMAZr and H_2O as the Hf, Zr, and O precursors, respectively. The Hf:Zr ratio are controlled by the cycle ratio of Hf and Zr precursors (here, Hf:Zr=1:1 for FE capacitors and Hf:Zr=1:3 for AFE capacitors). The samples were annealed at 500 °C in N_2 for 1 min by rapid thermal annealing.

Results and Discussion

Fig. 1 shows the TEM and EDS images of an AFE WN/HZO/WN structure. EDS data shows clear boundary between WN and HZO, indicating no obvious inter-diffusion. Fig. 2 shows the XRD measurements on FE and AFE HZO, with a tetragonal structure for Hf:Zr=1:3 and orthorhombic structure for Hf:Zr=1:1 after annealing [2]. Fig. 3 shows the P-E characteristics of FE WN/HZO/WN capacitors with thicknesses from 15 nm down to 4 nm. Fig. 4 shows the P-E characteristics of AFE WN/HZO/WN capacitors with thicknesses from 20 nm down to 4.5 nm. Clear FE and AFE hysteresis loops are achieved. Fig. 5 shows the P-V data of (a) a FE WN/HZO/WN capacitor with 4 nm HZO and (b) AFE WN/HZO/WN capacitor with 4.5 nm HZO. The corresponding thickness-dependent C-V data at 10 kHz for both FE and AFE capacitors are shown in Fig. 6(a) and Fig. 6(b). FE HZO exhibits typical two capacitance peaks while the AFE HZO exhibits four capacitance peaks. Fig. 7(a) shows the I-V characteristics of the AFE WN/HZO/WN capacitors. The AFE WN/HZO/WN capacitor has a sudden thickness dependence, as can be seen that current density increases by more than five orders of magnitude when thickness reduces from 4.5 nm to 4 nm, probably due to the much larger grain size and sharper grain boundaries, as shown in Fig. 8. This is the reason here why the ferroelectricity and anti-ferroelectricity are measured only down to 4 nm and 4.5 nm. The large leakage currents prevent us from obtaining reliable P-V and C-V data on even thinner HZO structures, although HZO capacitors with thickness of 1-3 nm were all fabricated and studied. We also realize that P-V loops obtained by piezo force microscopy (PFM) on 1-3 nm HZO structures are not reliable as the conclusive demonstration of ferroelectricity. The leakage current is found to be related with electrode materials and the Hf:Zr ratios, as shown in Fig. 7(b), indicating that they affect the crystallization process of HZO. Fig. 8(a) shows the TEM cross-sectional image of a 4 nm AFE HZO capacitor. Fig.8(b) and 8(c) show the zoom-in images of 4 nm and 4.5 nm AFE HZO, with the highlight of grain boundaries. The grain size of ~ 50 nm is found in 4 nm HZO (with a sharper grain boundary), which is significantly larger than that of 4.5 nm film with many smaller grains. We suspect that smaller crystalline grains mixed with amorphous HZO lead to much less leakage current in 4.5 nm or thicker films. Fig. 9 shows the P_S scaling metrics of AFE and FE HZO with WN electrodes. Fig. 10 shows the P_r scaling metrics of FE HZO with WN and TiN electrodes, confirming the HZO with WN has superior FE performance over TiN, especially at ultrathin film limit. Fig. 11 shows the dielectric constant scaling metrics of FE and AFE HZO with WN electrodes. A high dielectric constant of 30.4 is achieved with AFE WN/HZO/WN capacitor, with EOT of 0.62 nm and leakage of 3×10^{-7} A/cm^2 at 1 V. If operating with voltage range less than coercive voltage, the AFE HZO can be high performance high-k dielectrics considering both low leakage current and higher dielectric constant than both HfO_2 and ZrO_2. Fig. 12 shows the benchmark of (a) P_r versus thickness for FE HfO_2 and (b) P_S versus thickness for AFE HfO_2. Record high P_r on FE HZO and P_S on AFE HZO are achieved with WN electrodes in sub-10 nm regime, with a significantly larger P_r of 13.8 μC/cm^2 on 4 nm FE HZO and a large P_S of 28.1 μC/cm^2 on 4.5 nm AFE HZO.

The impact of scaling, Hf:Zr ratio and WN electrode on the polarization switching speed is further studied. Fig. 13 and Fig. 14 show the C-V measurements on FE and AFE capacitors with 6 nm HZO. A large frequency dispersion is observed in FE HZO. In great contrast, the frequency dispersion in AFE HZO is almost negligible. Fig. 15 shows the thickness-dependent frequency dispersion, characterized by C(1 MHz)/C(10 kHz), at maximum voltage applied on both AFE and FE HZO. It is clear that thinner film has slightly larger frequency dispersion and FE has much larger dispersion than AFE. The larger dispersion is associated with the time-response of HZO thin film, because at high frequency the dipoles inside HZO cannot response fast enough to achieve the same dielectric polarization as at low frequency. The dynamics of polarization switching are also characterized by pulse I-V measurements, as shown in Fig. 16. The FE HZO shows two peaks while the AFE HZO has four peaks, corresponding to two and four polarization switching events. Figs. 17 and 18 show the frequency-dependent P-V measurement on 4.5 nm thick FE and AFE HZO capacitors. P_S degradation in AFE HZO is much smaller than in FE HZO. Fig. 19 and Fig. 20 show the P_S versus frequency at different HZO thicknesses on both FE and AFE HZO capacitors. AFE HZO responses faster than FE HZO and remains up to MHz, in agreement with the results from C-V frequency dispersion. The real time response limit for AFE HZO needs to be further investigated.

Conclusion

In summary, the FE and AFE properties of HZO are investigated systematically down to 3 nm. The ferroelectric polarization, switching speed and the impact of WN electrodes are systematically studied. WN electrodes are found to improve the FE performance of HZO significantly with record high polarization charge density at the scaling limit. AFE HZO responses faster than FE HZO, suggesting AFE-FET could be more promising for high-speed memory devices. The work was partly supported by SRC and DARPA.

Reference [1] T. S. Boscke *et al.*, *APL*, p. 102903, 2011. [2] J. Muller *et al.*, *Nano Lett.*, p. 4318, 2012. [3] J. Muller *et al.*, *IEEE EDL*, p. 185, 2012. [4] S. Dunkel *et al.*, *IEDM*, p. 485, 2017 [5] W. Chung *et al.*, *VLSI*, p. T89, 2018. [6] N. Gong *et al.*, *IEEE EDL*, p. 1123, 2016. [7] Y.-C. Chiu *et al.*, *VLSI*, p. T185, 2015. [8] K. Ni *et al.*, *IEEE TED*, p. 2461, 2018. [9] M. Park *et al.*, *APL*, p. 242905, 2013. [10] X. Tian *et al.*, *APL*, p. 102902, 2018. [11] S. Muller *et al.*, *Adv. Funct. Mater.*, p. 2412, 2012. [12] M. H. Park *et al.*, *Adv. Mater.*, p. 1811, 2015. [13] T. S. Boscke *et al.*, *APL*, p. 112904, 2011. [14] K. D. Kim *et al.*, *Nano Energy*, p. 390, 2017. [15] E. Yurchuk *et al.*, *Thin Solid Films*, p. 88, 2013. [16] P. D. Lomenzo *et al.*, *APL*, p. 242903, 2015. [17] S. Muller *et al.*, *ECS J. Solid State Sci. Technol.*, p. N123, 2012. [18] S. Riedel *et al.*, *AIP Adv.*, p. 095123, 2016. [19] U. Schroeder *et al.*, *Inorg. Chem.*, p. 2752, 2018. [20] F. Ali *et al.*, *JAP*, p. 144105, 2017. [21] J. Müller *et al.*, *ICSSDM*, p. 1150, 2015.

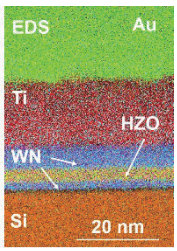

Fig. 1. TEM images and EDS analysis on AFE HZO capacitor.

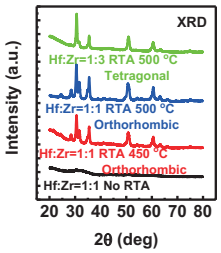

Fig. 2. XRD spectrum on FE and AFE HZO and the impact of annealing.

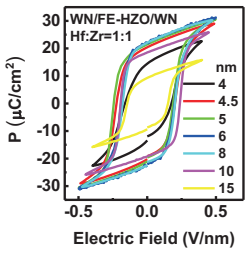

Fig. 3. P-E hysteresis loop of FE WN/HZO/WN with Hf:Zr=1:1 and different thicknesses.

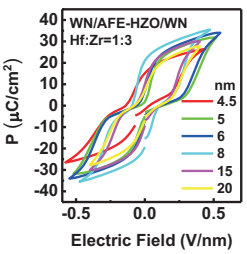

Fig. 4. P-E hysteresis loop of AFE WN/HZO/WN with Hf:Zr=1:3 and different thicknesses.

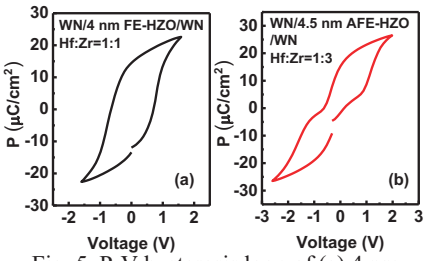

Fig. 5. P-V hysteresis loop of (a) 4 nm FE HZO with WN electrodes and Hf:Zr=1:1, (b) 4.5 nm AFE HZO with WN electrodes and Hf:Zr=1:3.

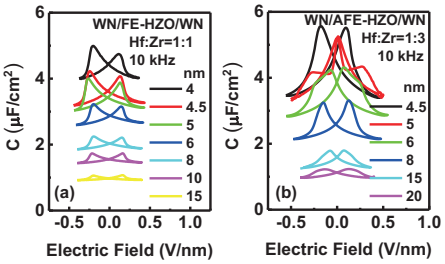

Fig. 6. C-V characteristics of FE WN/HZO/WN with (a) Hf:Zr=1:1 (b) Hf:Zr=1:3 and different thicknesses.

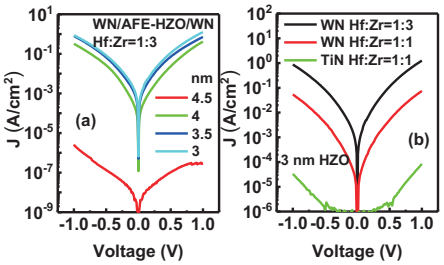

Fig. 7. I-V characteristics of (a) AFE WN/HZO/WN with Hf:Zr=1:3 and thicknesses down to 3 nm, (b) 3 nm HZO with different electrodes and Hf:Zr ratio.

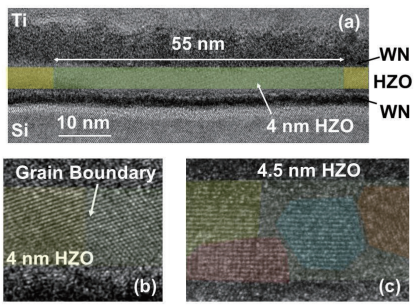

Fig. 8. False-color TEM cross-sectional images on AFE HZO. (a) 4 nm HZO (grain size > 50 nm), (b) zoom-in image of 4 nm HZO with sharp grain boundary and (c) 4.5 nm HZO showing much smaller grain size.

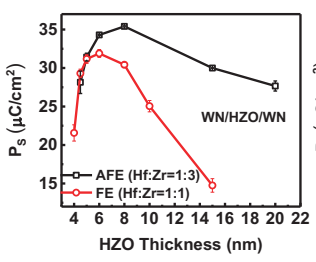

Fig. 9. P_S scaling metrics of AFE and FE HZO with WN electrodes.

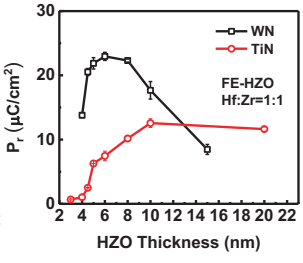

Fig. 10. P_r scaling metrics of FE HZO with WN and TiN electrodes.

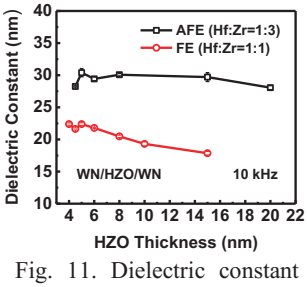

Fig. 11. Dielectric constant by C-V measurement scaling metrics of AFE and FE HZO with WN electrodes.

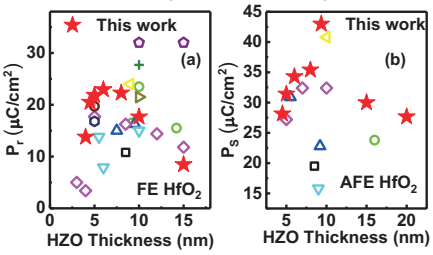

Fig. 12. Benchmark of (a) P_r vs. thickness of FE HfO_2 [1,9,10,12,13,16-19,21] and (b) P_S vs. thickness of AFE HfO_2 [1,11-14,20].

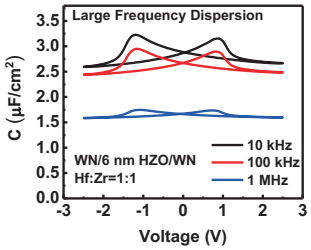

Fig. 13. C-V characteristics of 6 nm FE HZO with WN electrodes and Hf:Zr=1:1, showing large frequency dispersion.

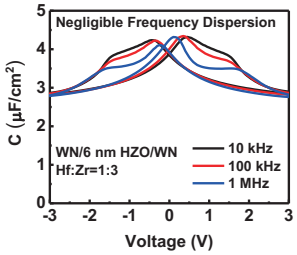

Fig. 14. C-V characteristics of 6 nm AFE HZO with WN electrodes and Hf:Zr=1:3, showing negligible frequency dispersion at high field.

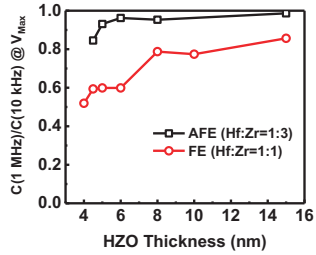

Fig. 15. Capacitance ratio of 1 MHz and 10 kHz at different thicknesses of both AFE and FE HZO.

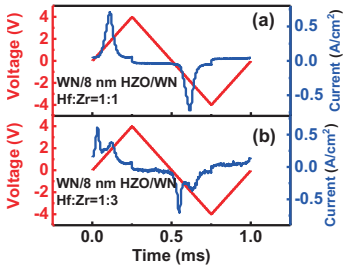

Fig. 16. Ramp pulse I-V measurements of (a) FE and (b) AFE HZO with WN electrodes and 8 nm HZO.

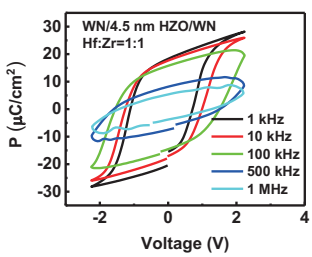

Fig. 17. Frequency-dependent P-V data of 4.5 nm FE HZO with WN electrodes and Hf:Zr=1:1 from ramp pulse I-V measurement.

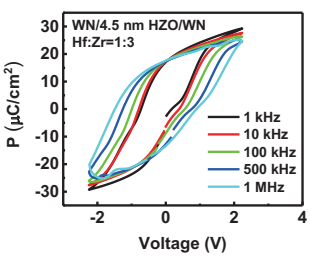

Fig. 18. Frequency-dependent P-V data of 4.5 nm AFE HZO with WN electrodes and Hf:Zr=1:3.

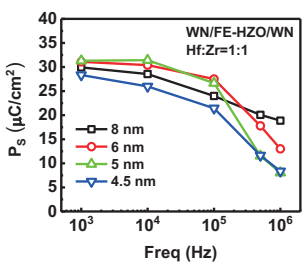

Fig. 19. P_S vs. frequency of FE WN/HZO/WN with Hf:Zr=1:1 and different HZO thicknesses.

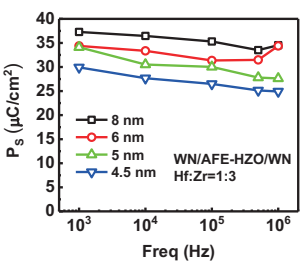

Fig. 20. P_S vs. frequency of AFE WN/HZO/WN with Hf:Zr=1:3 and different HZO thicknesses.